

Bias and Random Errors in Single Pixel Interrogation

S. Wereley, C. Meinhart, D. Tretheway, L. Gui, A. Sud

Abstract Recently a new μ PIV interrogation algorithm has been proposed in which the interrogation window size is reduced to a single pixel. Such small interrogation window sizes are possible using correlation averaging to increase the effective particle concentration to levels required for correlation analysis to succeed. The random error exhibits the expected behavior of decreasing roughly in proportion to $N^{-1/2}$ while the bias error exhibits unexpected peak-locking behavior with zero bias error at integer and half integer pixel displacements and maximal errors at one-quarter and three-quarter pixel displacements. Accompanying experiments show the potential of this technique but have not yet been sufficiently refined to confirm this unexpected bias error behavior.

1

Introduction

Particle Image Velocimetry (PIV) can be used to obtain high spatial resolution 2-D velocity fields. Santiago, et al. (1998) developed a μ PIV system capable of measuring slow flows—velocities on the order of millimeters per second—with a spatial resolution of $6.9 \times 6.9 \times 1.5 \mu\text{m}$. The system used an epi-fluorescent microscope and an intensified CCD camera to record 300 nm diameter polystyrene flow-tracing particles. The particles are illuminated at two instants in time using a continuous Hg-arc lamp. The velocity field is then deduced at many points within the field of view by using the cross correlation function and subpixel peak fitting to determine how the particles have moved during the time between the two illuminations. The continuous Hg-arc lamp is chosen for situations that require low levels of illumination light (e.g. flows containing living biological specimens) and where the velocity is sufficiently small so that the particle motion can be frozen by the CCD camera's electronic shutter.

Later applications of the μ PIV technique moved steadily toward faster flows more typical of aerospace applications. The Hg-arc lamp was replaced with a New Wave two-headed Nd:YAG laser that allowed cross correlation analysis of singly-exposed image pairs acquired with sub-microsecond time steps between images. The maximum velocity measurable with this time step is on the order of tens of meters per second. Meinhart, et al., (1999) applied μ PIV to measure the flow field in a $30 \mu\text{m}$ high \times $300 \mu\text{m}$ wide rectangular channel, with a flow rate of $50 \mu\text{l/hr}$, equivalent to a centerline velocity of 10 mm/s . The experimental apparatus, shown in Figure 1, images the flow with a $60\times$, $\text{NA}=1.4$, oil-immersion lens. The 200 nm diameter polystyrene flow-tracing particles were chosen small enough so that they faithfully followed the flow and were 150 times smaller than the smallest channel dimension. Wereley and Meinhart (2001) improved PIV accuracy while a subsequent investigation by Meinhart and Zhang (2000) of the flow inside a microfabricated ink jet printer head yielded the highest speed measurements made with μ PIV. Using a slightly lower magnification ($40\times$) and consequently lower spatial resolution, measurements of velocities as high as 8 m/s were made.

Because of the relatively low particle loading permitted by the volume illumination typically used in μ PIV, Correlation averaging has become a common method for increasing the Signal-to-Noise ratio in steady, quasi-steady and periodic microflow applications (Delnoij, et al., 1999; Meinhart, et al., 2000). The increased effective particle image concentration afforded by the correlation averaging allows for reducing the interrogation window size. In situations where it is possible to acquire very large data sets, thousands of images, the correlation region can be reduced to a single pixel (Westerweel, et al. 2004), herein denoted *SPE* to indicate 'single pixel evaluation'. Because cross correlation PIV depends on a 3 (or more) point correlation peak fit to reach subpixel accuracy, the way in which the cross correlation function is calculated must be completely changed. This change is shown schematically in Figure 2. In Figure 2a a spatially-averaged cross correlation function Φ_{spavg} is calculated from an ensemble pairs of images (only two shown in figure) using

S. Wereley, A Sud, Mechanical Engineering, Purdue University; C Meinhart, Env. and Mech. Eng, UCSB, D. Tretheway, Mech. Eng., Portland State Univ., L. Gui, NCPA, Univ. Miss.

$$\Phi_{spavg}(i, j; m, n) = \sum_{k=1}^{k_{tot}} \sum_{j=1}^q \sum_{i=1}^p f_k(i, j) \cdot g_k(i+m, j+n).$$

Generally this equation is not used directly but rather is accelerated using the FFT algorithm. In the single pixel version of this algorithm, the correlation function Φ_{spe} must be calculated in a neighborhood larger than one pixel in order to allow the peak fit for subpixel accuracy. This is done according to

$$\Phi_{spe}(i, j; m, n) = \sum_{k=1}^{k_{tot}} f_k(i, j) \cdot g_k(i+m, j+n)$$

where i and j are treated as parameters and allowed to vary over a large enough region to capture the correlation peak and allow the subpixel fit. Since this algorithm is in its infancy, not much is known about its possibilities and limitations. This paper will explore those limits using both simulated data sets as well as large experimental data sets.

2 Simulations

Two distinct flow profiles, simple shear and pressure-driven, were simulated using EDPIV, a PIV package especially well-suited for μ PIV, written by Lichuan Gui. Using these ideal simulated particle images, the behavior of the SPE algorithm can be explored. The simulated images allow for easy manipulation of particle diameter, concentration, and brightness, flow type and flow magnitude. Furthermore because the exact velocity field is known, simulated particle images provide an excellent opportunity for quantifying how PIV errors depend on the previously mentioned parameters. For example, PIV bias errors and peak locking have been studied using simulated image sets. In these simulated images two different flow types were simulated, a simple shear (or Couette) flow and a pressure-driven (or Poiseuille) flow.

Simple shear flow

The simple shear flow was simulated with displacements (the product of velocity and time in pixel units) ranging from -3 pixels to +3 pixels over a distance of 128 pixels. Two different particle image sizes were used, 3 pixels and 1 pixel. Figures 3 through 5 are organized such that the error or relative error (error divided by known displacement) is plotted on the vertical axis and the displacement is plotted on the horizontal axis. This type of plot will reveal if the error depends on the displacement being measured—a phenomenon called ‘peak locking’ or ‘pixel locking’. In conventional spatially-averaged correlation PIV, the 1 pixel diameter particle images would be expected to exhibit considerable peak locking. Figure 3 shows the total error for 3 pixel diameter particle images, for two data sets—one with 1000 images and one with 10000 images. In both cases it is evident that the error is dominated by the random error and there is no evidence of any bias error. According to statistical theory, a random noise signal should vary in proportion to $N^{1/2}$ where N is a large number of samples. This is approximately the reduction in noise observed in Figure 3. Figure 4 on the other hand shows the difference between unshifted and shifted interrogation windows for 1000 image pairs with 1 pixel diameter particle images. The errors are again dominated by the random error and there is no noticeable difference between Figure 4a and 4b. Particle images this small typically cause substantial peak locking in spatially-averaged correlation schemes. Comparing Figure 4 to Figure 3, there is no evidence of an increase in the level of peak locking when the particle size is reduced from 3 pixels to 1 pixel. In fact, there is no evidence of any peak locking at all in either case. In both cases the mean is nearly zero and the standard deviation is approximately 0.005 pix. In spatially-averaged correlation, the bias errors in the algorithm increase with increasing displacements. No evidence of this type of behavior is apparent here. Comparing the shifted and unshifted correlation windows shows that for single pixel evaluation, window shifting is unnecessary.

Pressure-driven flow

Two different pressure-driven flows were simulated, one with a maximal (i.e. centerline) displacement of 2 pixels and one with a maximal displacement of 5 pixels. For both pressure-driven flows, the same particle image properties as above were used. Because of the curvature of the pressure-driven flow, we would expect some bias errors in the measurement. Figure 5a and 5b show the results of simulations using a 2 pixel and 5 pixel maximal displacement, respectively. These figures show unexpected behavior, namely that the error is minimized (in an absolute sense) for integer and half integer displacements while it is maximized for quarter and three-quarter pixel

displacements. In conventional spatially-averaged correlation PIV, the error is minimized at integer pixel displacements and maximized at half pixel displacements. This behavior is evident in both Figure 5a and 5b, 2 and 5 pixel displacement, meaning that it is not a result of a particular choice of maximal displacement. It is possible that this error behavior is related to how the simulated particle images are generated, although this is not likely because both this type of simulation technique as well as this particular implementation have been widely used in the past to study bias errors. We will look to the experiments for support for this error pattern.

3 Experiments

μ PIV was used to measure a laminar flow through a $30 \times 300 \mu\text{m}$ glass microchannel, manufactured by *Wilmad Industries*. The flow was seeded by 200 nm diameter flow-tracing polystyrene particles. The fluorescent particles were excited by the two pulsed Nd:YAG lasers, imaged using an $M = 60$, $NA = 1.4$ oil-immersion objective lens, and recorded by a Princeton Instruments 1300×1030 pixel \times 12 bit cooled interline-transfer CCD camera. The microchannel experiment is described in further detail by Meinhart, et al. (1999).

A $30 \mu\text{m} \times 300 \mu\text{m} \times 25$ mm glass rectangular microchannel, fabricated by *Wilmad Industries*, was mounted flush to a $170 \mu\text{m}$ thick glass coverslip and a microscope slide (see Figure 6). By carefully rotating the glass coverslip and the CCD camera, the channel was oriented to the optical plane of the microscope within 0.2° , in all three angles. The orientation was confirmed optically by focusing the CCD camera on the microchannel walls. The microchannel was horizontally positioned using a high-precision x - y stage, and verified optically to within ~ 400 nm using epi-fluorescent imaging and image enhancement.

The glass microchannel was imaged through an inverted epi-fluorescent microscope and a *Nikon Plan Apochromat* oil-immersion objective lens with a magnification $M = 60$ and a numerical aperture $NA = 1.4$. The object plane was placed at approximately $7.5 \pm 1 \mu\text{m}$ from the bottom of the $30 \mu\text{m}$ thick microchannel. The Plan Apochromat lens was chosen for the experiment, because it is a high quality microscope objective designed with low curvature of field, low distortion, and corrected for spherical and chromatic aberrations (Inoué & Spring, 1997).

Since deionized water was used as the working fluid, the effective numerical aperture of the objective lens was limited to $NA \approx 1.23$. A filtered continuous white light source was used to align the test section with the CCD camera and to test for proper particle concentration. During the experiment, the continuous light source was replaced by the pulsed Nd:YAG laser. A *Harvard Apparatus* syringe pump was used to produce a $200 \mu\text{l hr}^{-1}$ flow through the microchannel.

In our previous work, the particle images were analyzed using a Matlab-based PIV interrogation program developed specifically for microfluidic applications. The program uses an ensemble-averaging correlation technique to estimate velocity vectors at a single measurement point by (1) cross correlating particle-image fields from twenty instantaneous realizations, (2) averaging those cross correlation functions, and (3) determining the peak location of the averaged correlation function. This process is repeated for each velocity vector in the measurement domain. For these previous experiments, twenty realizations were chosen because that was more than a sufficient number of realizations to give excellent signal, even with a first interrogation window of only 120×8 pixels.

In spatially-averaged cross correlation PIV, the spatial resolution of the velocity measurements is the size of the first interrogation window plus the displacement being measured. Since the interrogation window is much larger than the displacement in this case, the spatial resolution is approximately equal to the first interrogation window—or $13.6 \times 0.9 \mu\text{m}$ in-plane and $1.8 \mu\text{m}$ out-of-plane. Based on this interrogation window size and using 50% overlap between neighboring windows, five thousand time-averaged velocity measurements were obtained over the whole image. The velocity vectors closest to the wall are shown in Figure 4. The signal-to-noise ratio resulting from the ensemble-average correlation technique was high enough that there were no erroneous velocity measurements. Consequently, no vector validation was performed on the data after interrogation. The velocity field was smoothed using a 3×3 Gaussian kernel with a standard deviation of 1 grid spacing in both directions.

Since the microchannel flow was fully developed, the wall-normal component of the velocity vectors should be close to zero. The average angle of inclination of the velocity field was found to be small, 0.0046 radians, suggesting that test section was slightly rotated relative to the CCD array. This was corrected mathematically by rotating the coordinate system of the velocity field by 0.0046 radians. The precise location of the wall was more accurately determined by applying the no-slip boundary condition and extrapolating the velocity profile to zero at 16 different streamwise positions (see Figure 7). The location of the wall at every streamwise position agreed to within

8 nm of each other, suggesting that the wall is extremely flat, the optical system has little distortion, and the PIV measurements are very accurate.

These experiments were repeated using similar experimental parameters, flow rate, channel size, particle size and concentration, etc., except that many more images were acquired to allow for single pixel evaluation. The previous experiments indicate that 20 image pairs generated a sufficient signal-to-noise ratio that very good measurements could be made using a 120×8 pixel interrogation region, or effectively, $120 \times 8 \times 20 = 19200$ pixels total. Camera and computer architecture limited the size of the single pixel data set to 1000 image pairs which translates to $1 \times 1 \times 1000 = 1000$ pixels total. The signal-to-noise ratio of these measurements could be expected to be somewhat lower since the measurement is based on only 5% of the number of pixels used for the spatially-averaged measurements. Still, that factor of 20 should increase the noise level by about a factor of 4. The results of the single pixel evaluation are shown in Figure 8. The higher noise level is quite evident as are a number of missing vectors where no particles happened to occur in any of the image pairs acquired. Despite these problems the results are encouraging and would be even better if a fair comparison using 20000 image pairs were made. Work is underway to get around the constraint to 1000 images.

4

Conclusions

The single pixel evaluation algorithm in which the interrogation window size is reduced to a single pixel has been evaluated both computationally and experimentally. In the simulations the random error was found to exhibit the expected behavior of decreasing roughly in proportion to $N^{-1/2}$ while the bias error exhibits unexpected peak-locking behavior with zero bias error at integer and half integer pixel displacements and maximal errors at one-quarter and three-quarter pixel displacements. The accompanying experiments show the potential of this technique but have not yet been sufficiently refined to confirm the unexpected bias error behavior observed in the simulations.

Acknowledgements

The authors wish to acknowledge the support of the National Science Foundation, grant 0426779-CTS.

References

- Delnoij E, Westerweel J, Deen NG, Kuipers JAM, Van Swaaij WPM** (1999) Ensemble correlation PIV applied to bubble plumes rising in a bubble column. *Chem Eng Sci* 54:5159–5171.
- Meinhart CD, Wereley ST, Santiago JG** (2000) A PIV algorithm for estimating time-averaged velocity fields. *J Fluids Eng* 122:285–289.
- Santiago JG, Wereley ST, Meinhart CD, Beebe DJ, Adrian RJ** (1998) A particle image velocimetry system for microfluidics. *Exp. Fluids* 25, 316-319.
- Meinhart CD and Zhang H** (2000) The flow structure inside a microfabricated inkjet printer head, *J. Microelectromechanical Systems*, Vol. 9, 67-75.
- Meinhart CD, Wereley ST, Santiago JG** (1999) PIV measurements of a microchannel flow, *Exp. Fluids*, Vol. 27, 414-419.
- Wereley ST and Meinhart CD** (2001) Second-Order Accurate Particle Image Velocimetry,” *Exp. Fluids*, Vol. 31, 258-268.
- Westerweel J, Geelhoed PF, Lindken R** (2004) Single-pixel resolution ensemble correlation for micro-PIV applications, *Exp. Fluids*, Vol. 37, 375-384.

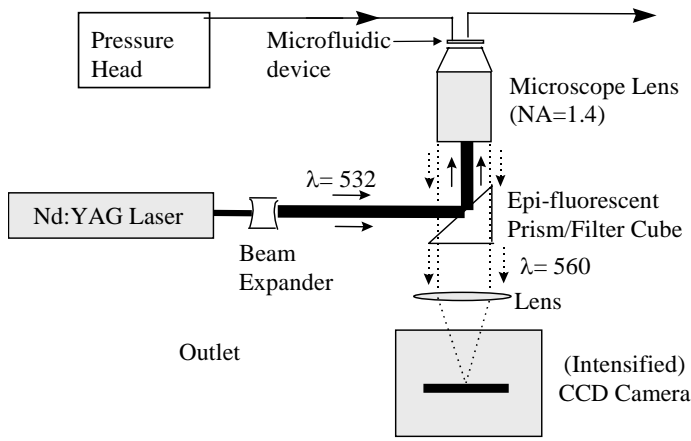


Figure 1. Diagram of typical μ PIV system.

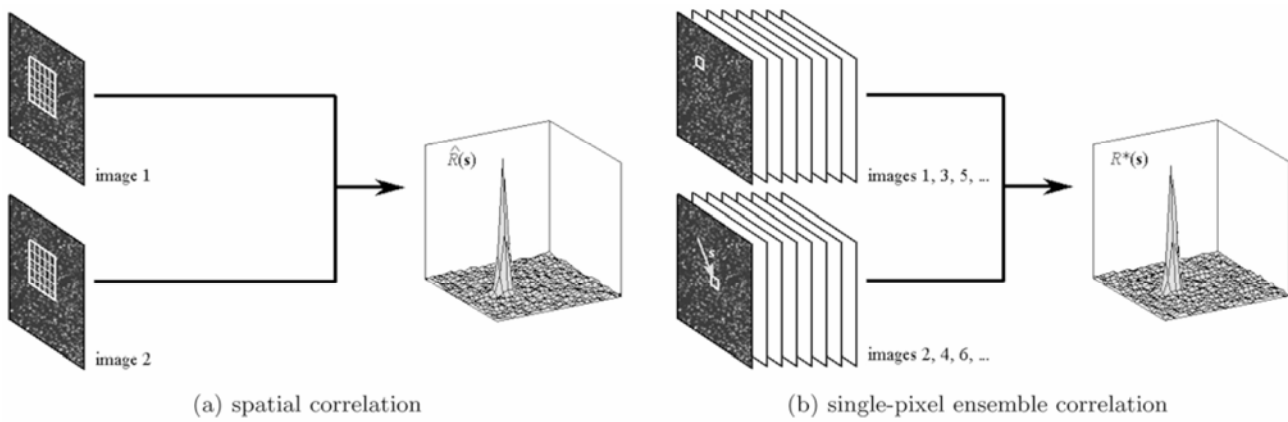


Figure 2. Schematic comparison of (a) spatially-averaged cross correlation algorithm (customary) compared to (b) the Single Pixel Evaluation algorithm (Westerweel, et al., 2004).

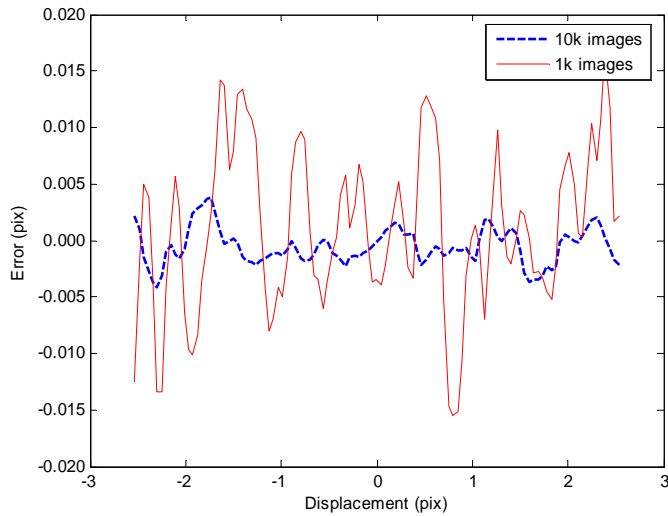


Figure 3. Error as a function of displacement for image sets of 10000 image pairs and 1000 image pairs.

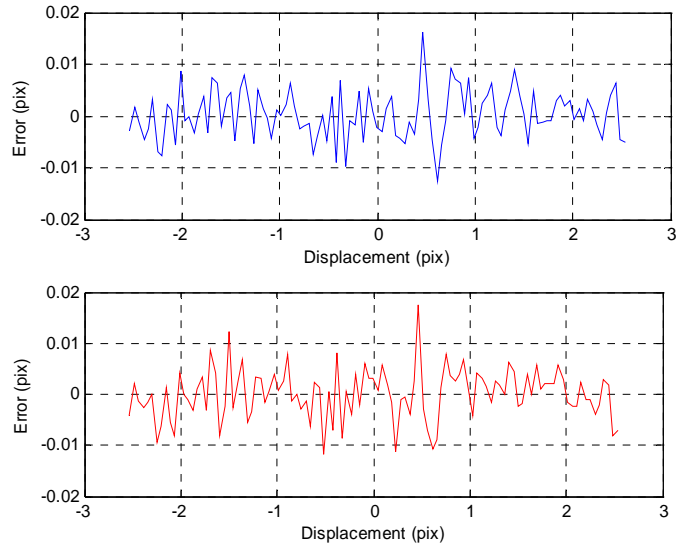


Figure 4. Comparison of unshifted (a) and shifted (b) results.

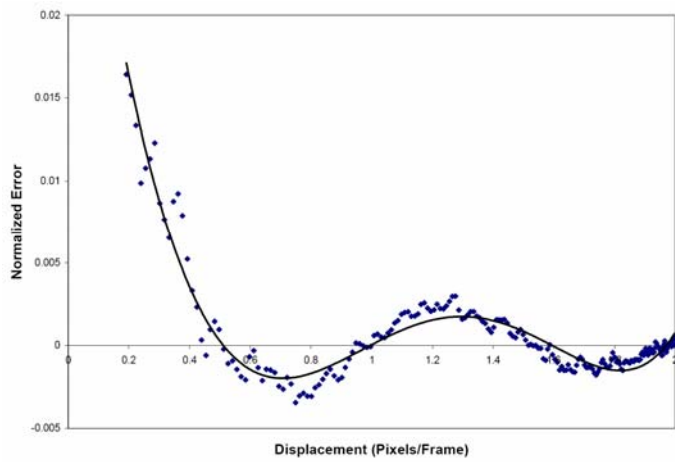


Figure 5a. Error versus displacement plot for 2 pixel maximal displacement pressure-driven flow.

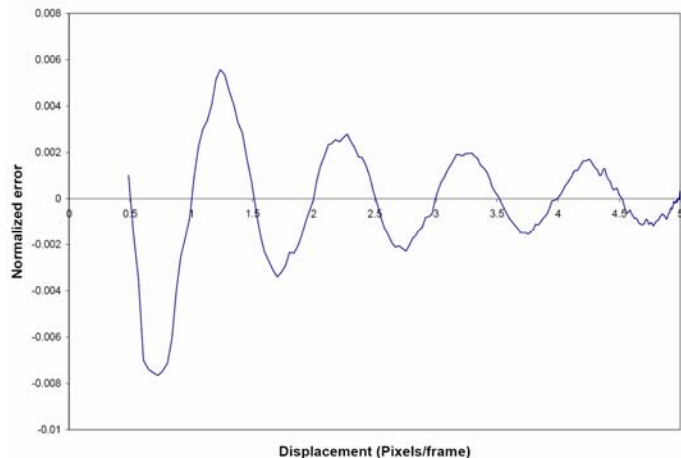


Figure 5b. Error versus displacement plot for 5 pixel maximal displacement pressure-driven flow.

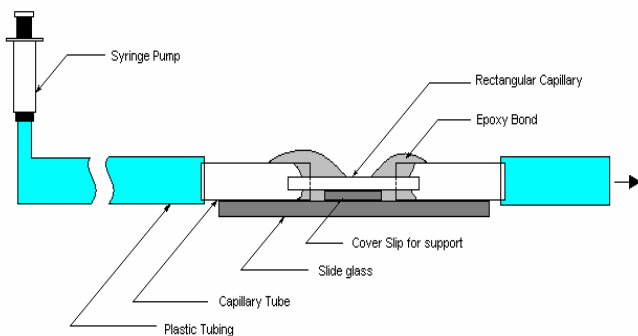


Figure 6. Detail of the nominally $30\ \mu\text{m} \times 300\ \mu\text{m}$ rectangular glass microchannel, which is glued to a circular capillary tube and a $170\ \mu\text{m}$ glass coverslip for support. Plastic tubing connects the capillary tube to the syringe pump.

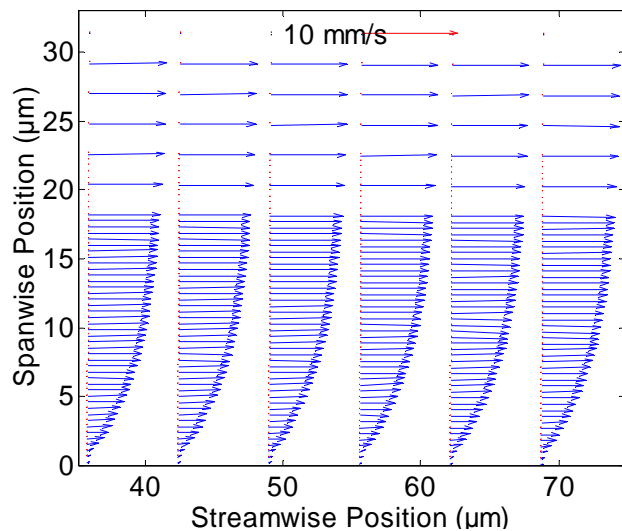


Figure 7. Correlation-averaged velocity-vector field measured in a $30\ \mu\text{m}$ deep \times $300\ \mu\text{m}$ wide \times $25\ \text{mm}$ long channel. The spatial resolution $13.6\ \mu\text{m} \times 0.9\ \mu\text{m}$ near the wall. A 50% overlap between interrogation spots yields a velocity vector spacing of $450\ \text{nm}$ in the spanwise direction near the wall.

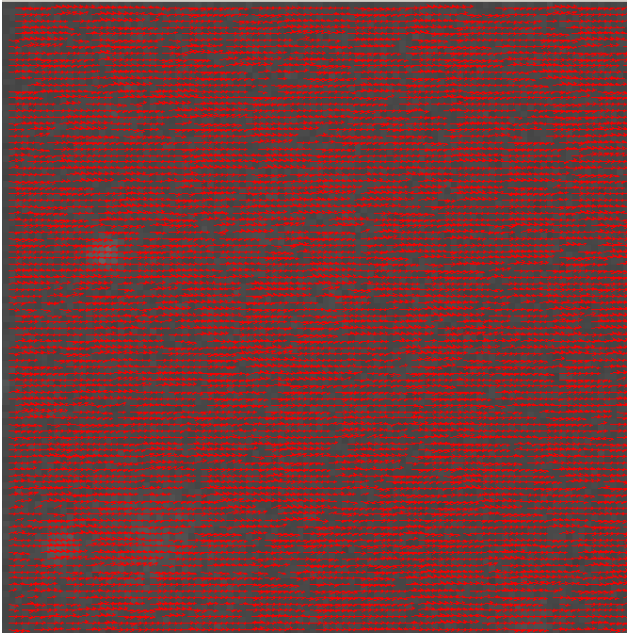


Figure 8. Single pixel evaluation of images. Notice the drop outs and somewhat higher random noise level than the spatially-averaged results shown in Figure 7.